Luminescent silicon nanoparticles prepared by ultra short pulsed laser ablation in liquid for imaging applications

R. Intartaglia,[*] **K. Bagga, M. Scotto, A. Diaspro, and F. Brandi**

Department of Nanophysics, Istituto Italiano di Tecnologia, via Morego, 30, 16163 Genova, Italy
[*]romuald.intartaglia@iit.it

Abstract: Heavy-metal-free semiconductor material like Silicon Nanoparticle (Si-NPs) is attracting scientists because of their diverse applications in biomedical field. In this work, pulsed laser ablation of silicon in aqueous solution is employed to generate Si-NPs in one step avoiding use of chemical precursors. Characterization by absorption, electron and photoluminescence analysis proves the generation of luminescent Si-NPs. The productivity rate of Si-NPs is investigated by Inductively Coupled Plasma Spectrometry. Furthermore, Si-NPs quantum yield and confocal microscopy studies corroborate the potential use of these biocompatible Si-NPs for imaging applications.

References and links

1. K. Fujioka, M. Hiruoka, K. Sato, N. Manabe, R. Miyasaka, S. Hanada, A. Hoshino, R. D. Tilley, Y. Manome, K. Hirakuri, and K. Yamamoto, "Luminescent passive-oxidized silicon quantum dots as biological staining labels and their cytotoxicity effects at high concentration," Nanotechnology **19**(41), 415102 (2008).
2. M. De, P. S. Ghosh, and V. M. Rotello, "Applications of Nanoparticles in Biology," Adv. Mater. (Deerfield Beach Fla.) **20**(22), 4225–4241 (2008).
3. V. Rotello, *Nanoparticle: Building Blocks for Nanotechnology* (Springer, 2004), 300 pp.
4. F. Erogbogbo, K. T. Yong, I. Roy, R. Hu, W. C. Law, W. Zhao, H. Ding, F. Wu, R. Kumar, M. T. Swihart, and P. N. Prasad, "In vivo targeted cancer imaging, sentinel lymph node mapping and multi-channel imaging with biocompatible silicon nanocrystals," ACS Nano **5**(1), 413–423 (2011).
5. F. Erogbogbo, K. T. Yong, R. Hu, W. C. Law, H. Ding, C. W. Chang, P. N. Prasad, and M. T. Swihart, "Biocompatible magnetofluorescent probes: luminescent silicon quantum dots coupled with superparamagnetic iron(III) oxide," ACS Nano **4**(9), 5131–5138 (2010).
6. Z. F. Li and E. Ruckenstein, "Water-Soluble Poly(acrylic acid) Grafted Luminescent Silicon Nanoparticles and Their Use as Fluorescent Biological Staining Labels," Nano Lett. **4**(8), 1463–1467 (2004).
7. J. W. Aptekar, M. C. Cassidy, A. C. Johnson, R. A. Barton, M. Lee, A. C. Ogier, C. Vo, M. N. Anahtar, Y. Ren, S. N. Bhatia, C. Ramanathan, D. G. Cory, A. L. Hill, R. W. Mair, M. S. Rosen, R. L. Walsworth, and C. M. Marcus, "Silicon nanoparticles as hyperpolarized magnetic resonance imaging agents," ACS Nano **3**(12), 4003–4008 (2009).
8. L. Xiao, L. Gu, S. B. Howell, and M. J. Sailor, "Porous silicon nanoparticle photosensitizers for singlet oxygen and their phototoxicity against cancer cells," ACS Nano **5**(5), 3651–3659 (2011).
9. D. Kovalev and M. Fujii, "Silicon Nanocrystals: Photosensitizers for Oxygen Molecules," Adv. Mater. (Deerfield Beach Fla.) **17**(21), 2531–2544 (2005).
10. M. Rosso-Vasic, E. Spruijt, Z. Popovic, K. Overgaag, B. Van Lagen, B. Grandidier, D. Vanmaekelbergh, D. Dominguez-Gutierrez, L. De Cola, and H. Zuilhof, "Amine-terminated silicon nanoparticles: synthesis, optical properties and their use in bioimaging," J. Mater. Chem. **19**(33), 5926–5933 (2009).
11. X. Zhang, D. Neiner, S. Wang, A. V. Louie, and S. M. Kauzlarich, "A new solution route to hydrogen-terminated silicon nanoparticles: synthesis, functionalization and water stability," Nanotechnology **18**(9), 095601 (2007).
12. Y. Khang and J. Lee, "Synthesis of Si nanoparticles with narrow size distribution by pulsed laser ablation," J. Nanopart. Res. **12**(4), 1349–1354 (2010).
13. J. Knipping, H. Wiggers, B. Rellinghaus, P. Roth, D. Konjhodzic, and C. Meier, "Synthesis of high purity silicon nanoparticles in a low pressure microwave reactor," J. Nanosci. Nanotechnol. **4**(8), 1039–1044 (2004).
14. S. Barcikowski, F. Devesa, and K. Moldenhauer, "Impact and structure of literature on nanoparticle generation by laser ablation in liquids," J. Nanopart. Res. **11**(8), 1883–1893 (2009).

15. R. Intartaglia, K. Bagga, F. Brandi, G. Das, A. Genovese, E. Di Fabrizio, and A. Diaspro, "Optical Properties of Femtosecond Laser-Synthesized Silicon Nanoparticles in Deionized Water," J. Phys. Chem. C **115**(12), 5102–5107 (2011).
16. R. Intartaglia, A. Barchanski, K. Bagga, A. Genovese, G. Das, P. Wagener, E. Di Fabrizio, A. Diaspro, F. Brandi, and S. Barcikowski, "Bioconjugated silicon quantum dots from one-step green synthesis," Nanoscale **4**(4), 1271–1274 (2012).
17. K. Abderrafi, R. García Calzada, M. B. Gongalsky, I. Suárez, R. Abarques, V. S. Chirvony, V. Y. Timoshenko, R. Ibáñez, and J. P. Martínez-Pastor, "Silicon Nanocrystals Produced by Nanosecond Laser Ablation in an Organic Liquid," J. Phys. Chem. C **115**(12), 5147–5151 (2011).
18. V. Svrcek, D. Mariotti, and M. Kondo, "Ambient-stable blue luminescent silicon nanocrystals prepared by nanosecond-pulsed laser ablation in water," Opt. Express **17**(2), 520–527 (2009).
19. P. G. Kuzmin, G. A. Shafeev, V. V. Bukin, S. V. Garnov, C. Farcau, R. Carles, B. Warot-Fontrose, V. Guieu, and G. Viau, "Silicon Nanoparticles Produced by Femtosecond Laser Ablation in Ethanol: Size Control, Structural Characterization, and Optical Properties," J. Phys. Chem. C **114**(36), 15266–15273 (2010).
20. K. Sasaki and N. Takada, "Liquid-phase laser ablation," Pure Appl. Chem. **82**(6), 1317–1327 (2010).
21. G. Belomoin, J. Therrien, A. Smith, S. Rao, R. Twesten, S. Chaieb, M. H. Nayfeh, L. Wagner, and L. Mitas, "Observation of a magic discrete family of ultrabright Si nanoparticles," Appl. Phys. Lett. **80**(5), 841–843 (2002).
22. P. F. Trwoga, A. J. Kenyon, and C. W. Pitt, "Modeling the contribution of quantum confinement to luminescence from silicon nanoclusters," J. Appl. Phys. **83**(7), 3789–3794 (1998).
23. G. A. Crosby and J. N. Demas, "The measurement of photoluminescence quantum yields," J. Phys. Chem. **75**(8), 991–1024 (1971).
24. J. P. Zimmer, S. W. Kim, S. Ohnishi, E. Tanaka, J. V. Frangioni, and M. G. Bawendi, "Size series of small indium arsenide-zinc selenide core-shell nanocrystals and their application to in vivo imaging," J. Am. Chem. Soc. **128**(8), 2526–2527 (2006).
25. C. L. Sajti, R. Sattari, B. N. Chichkov, and S. Barcikowski, "Gram Scale Synthesis of Pure Ceramic Nanoparticles by Laser Ablation in Liquid," J. Phys. Chem. C **114**(6), 2421–2427 (2010).
26. A. Abdolvand, S. Z. Khan, Y. Yuan, P. L. Crouse, M. J. J. Schmidt, M. Sharp, Z. Liu, and L. Li, "Generation of titanium-oxide nanoparticles in liquid using a high-power, high-brightness continuous-wave fiber laser," Appl. Phys., A Mater. Sci. Process. **91**(3), 365–368 (2008).
27. T. Maldiney, G. Sraiki, B. Viana, D. Gourier, C. Richard, D. Scherman, M. Bessodes, K. Van den Eeckhout, D. Poelman, and P. F. Smet, "*In vivo* optical imaging with rare earth doped $Ca_2Si_5N_8$ persistent luminescence nanoparticles," Opt. Mater. Express **2**(3), 261–268 (2012).

1. Introduction

In the last decade, the rapid progress in nanoscale synthesis of materials has allowed the development of nanostructure for bio-medical applications. However, the potential success of these nanostructures in the clinical setting relies on consideration of important parameters, such as nanoparticle fabrication strategies, their physical properties and most importantly, minimum toxicity of the carrier itself. Heavy-metal-free semiconductor materials like nanoscale silicon (Si) have attracted scientists in nanoscience research because of their biocompatibility with respect to nanoparticles derived from non-biological materials [1] and for its diverse applications. The versatility of the applications of Si based nanostructures has been demonstrated in the biomedical field [2,3] such as in vivo fluorescence imaging label [4–6], bio imaging contrast agent [7] and therapy [8,9].

Up to now, several chemical [10,11] and physical methods [12,13] have been developed for the Silicon nanoparticle (Si-NPs) synthesis. Among them chemistry route has attracted more attention because this technique offers simultaneous control on particle size and surface properties which is required for NP functionalization. However, such techniques have the drawback of involving the use of chemical products and reducing agents [10,11] or require multi-step procedures for the NPs size control. It is important to develop a simple technique that may avoid these aspects. Recently, pulsed laser ablation in liquid (PLAL) has emerged as an alternative approach to generate pure nanoparticle colloidal solution [14,15]. PLAL has the advantages to be: i) a chemically clean synthesis, without the requirement of chemical precursors; ii) simple, since it is performed at ambient conditions, without the need of extreme temperature and pressure conditions; iii) versatile, since the obtained NPs are in colloidal solution form, giving the opportunity for further nanoscale manipulations, such as functionalization [16].

The production of Si-NPs colloidal solution via PLAL has been investigated for different pulse durations and laser wavelengths. Most of the studies report synthesis of Si-NPs via PLAL method using nanosecond laser pulses, resulting in NPs which stabilize into clusters [17,18]. Post-chemical treatment of the clusters is then required since most of the applications need non agglomerated nanoparticles. Recently, our group investigated the generation of Si-NPs by near-infrared femtosecond PLAL demonstrating a size control mechanism dependent on the laser pulse energy [15].

On the other hand, photoluminescence (PL) properties of Si-NPs produced by PLAL have been found to be strongly dependent of pulse duration and laser wavelength. Swerk *et al* have shown that the PL of Si-NPs is located near 400 nm [18]. Recently, luminescence measurements on Si-NPs prepared by PLAL displayed PL peak feature around 630 nm [19]. As a consequence, further investigations of the optical properties of the SiNP colloidal solutions obtained by PLAL are necessary in order to clarify a situation with very high biotechnological potentialities.

In this work, we prepared Si-NPs colloidal solution by PLAL technique and investigated their photoemissive properties for imaging applications. Si-NPs colloidal solution has been prepared in deionized water using femtosecond laser pulses in two regime of laser energy. These particles were characterized using absorption and photoluminescence spectroscopy (PL), transmission electron microscopy (TEM), fluorescence imaging microscopy. UV spectroscopy together with TEM analysis confirm the successful fabrication of Si-NPs with average size of 65 nm and 5 nm, characterized by a absorption peak at wavelength of 485 nm and 460 nm, respectively. Photoluminescence of the small and large Si-NPs colloidal solution is dominated by a blue and red band emission, respectively. The productivity of Si-NPs, i.e. number of generated nanoparticles, has been investigated by Inductively Coupled Plasma Optical Emission Spectrometry (ICP-OES). Finally, we have explored by fluorescence imaging microscopy the potential use of these nanoparticles for imaging applications.

2. Experimental section

The synthesis of pure Si nanoparticle was carried by femtosecond laser ablation in an aqueous solution as previously described [15,16]. The specific laser ablating conditions and instrumentation are summarized here. In brief, the laser system used in this study consisted of a Ti:sapphire laser with a pulse width of 110 fs centered at 800 nm operating at a repetition rate of 1 kHz. The laser beam is focused using a lens with a focal length of 10 cm onto the Si target (99.999% from Alpha Aesar) placed on the bottom of a quartz cuvette and immersed in 1 ml of liquid medium, deionized water. Before each experiment the target was mechanically polished and then washed with the same liquid used for the ablation several times to remove impurity from the surface. During laser ablation, the target was moved with a rotation system (T-cube DC Servo controller, Thor labs) to achieve uniform irradiation of the silicon surface. Size and distribution of Si-NPs synthesized using near-infrared femtosecond PLAL technique were demonstrated to depend on the laser pulse energy [15]. In particular, two distinct regime for size controlled Si-NPs generation has been revealed with a threshold energy of about 0.25 mJ pulse energy. In the low energy regime, 0.15mJ, the color of the solution is transparent, while it becomes light yellow in the high energy regime, 0.4mJ. All characterization measurements were performed 1 day after preparation of the colloidal solution.

Transmission electron microscopy (TEM) images were acquired on a JEOL Jem 1011 microscope working at an acceleration voltage of 100 KeV. High resolution transmission electron microscopy (HRTEM) analyses were performed on a JEOL Jem 2200FS microscope equipped with a field emission electron gun working at 200 KV. TEM samples were prepared by dropping the colloidal solution directly onto a carbon-coated 300 mesh copper grids and allowing the solution to evaporate at Normal Temperature and Pressure.

1 ml colloidal solution was used to measure the absorption and photoluminescence spectra. Optical absorption spectra were recorded in quartz cuvette (10 mm, Helma), using a

Cary 6000i UV-VIS spectrophotometer in double beam mode. The scan range was 200-1000 nm with a 600 nm/min rate. The photoluminescence (PL) measurements for colloidal solution were carried out in the 350-800 nm wavelength range by Fluoromax-4 Spectrofluorometer (Horiba-JobinYvon) fitted with a photomultiplier and a Xenon lamp source. PL and absorption spectra were corrected for solvent contribution.

Analytical productivity of Si-NPs, were evaluated by Inductively Coupled Plasma Optical Emission Spectrometry (ICP-OES), ICAP 6300 duo thermo scientific. For this measurement, 100 µl solution of Si-NPs was introduced in Aqua regia, and after overnight acid digestion the final volume was adjusted with Milli-Q water to 25 mL. The dilution factor is kept into consideration while determinating the final concentration.

Confocal imaging experiments have been performed using an inverted Nikon A1 microscope equipped with a 40x objective and with multiple laser lines. Spectral images have been acquired exciting at 405nm a drop of Si NPs casted on cover slide. The emitted fluorescence is then collected by the 40x objective and sent to a set of gratings and then to a multichannel photomultiplier tube. The optical path is designed to have a 6nm spectral resolution on each channel of the detector. The sample during the evaporation self organizes in coffee ring-like configuration; several images have been acquired on the edge of the coffee ring. To be noted, the material property of the sample in liquid and after the evaporation of excess liquid remains the same.

3. Results

3.1 Synthesis

Figure 1 shows respectively the TEM images of the particles in the colloidal solution obtained by femtosecond laser ablation in the (a) high, 0.4mJ and (b) low, 0.15mJ, energy regime. The mean and distribution sizes of particles obtained by counting more than 300 particles in the electron microscopy images are shown on the right of each corresponding microphotograph. In the high pulse energy regime isolated Si-NPs, i.e. non-agglomerated substrate-free NPs are observed along with SiOx amorphous matrix which is outcome of peculiarity of laser ablation technique, since temperature is locally high (around 5000 K) [20] and silicon oxidation occurs when silicon and water come into contact. The obtained colloidal solution displays an average size of 65 nm and a size distribution varying from 10 nm to 120 nm (Fig. 1(a)). In the low pulse energy regime, TEM analysis reveals a drastic particle size reduction as reported in Fig. 1(b). The obtained colloidal solution displays a average size of 5.5 nm and a size distribution varying from 1 nm to 8 nm. HRTEM imaging reveals that Si-NPs prepared by femtosecond PLAL technique display clearly the crystalline structure of Si bulk with an interplanary spacing of 3.12 Å, i.e., internal oxide free structure (inset of the Fig. 1(b)). Micro-Raman analysis showed also the presence of SiOx structure [15].
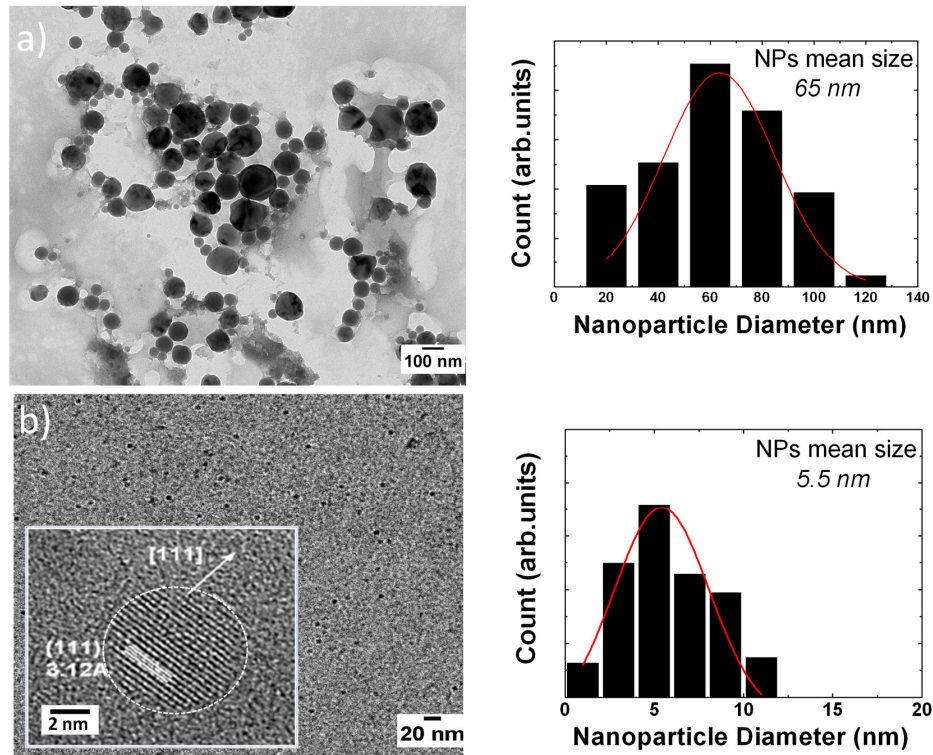
Fig. 1. TEM image of silicon nanoparticle colloidal solution prepared via femtosecond laser ablation in deionized water in two laser pulse regime (a) high and (b) low. On the right is reported the corresponding size histogram. A HRTEM image of a single Si-NP showing the (111) lattice sets is shown in the b) inset.

3.2 Optical properties

We were successful in fabricating different size distributions of Si-NPs in deionized water using PLAL technique. As a consequence, further investigations of the optical properties of the colloidal solutions obtained by PLAL of silicon are necessary in order to highlight the bio-technological potentialities. Figure 2 shows representative plots of absorption and photoluminescence spectra of the Si-NPs prepared via PLAL in deionized water. Figure 2(a) displays the UV-visible absorption measurement of the Si-NPs solution obtained in the high (red line) and low (blue line) energy regime. All absorption spectra appear to have a broad continuous band between 200 and 800 nm and a distinctive shoulder with a minimum absorbance at around 400 nm. For the clarity of the figure, the absorption spectra were normalized to 1 at the shoulder maximum peak value. The observation of characteristic absorption peak at wavelength of 485 nm and 460 nm for the colloidal solution proves the successful fabrication of Si-NPs with high and small average size, respectively [15]. Then, luminescence properties of Si-NPs prepared in water in both laser energy regime have been investigated. Figure 2(b) shows PL spectrum under 400 nm excitation wavelength for both Si colloidal solution. For clarity, the PL intensity of the colloidal solution prepared in the high energy regime is multiplied by a factor 10. For the colloidal solution prepared by PLAL in the lower energy regime, the Si-NPs colloidal solution displays stable PL emission, characterized by a blue-green emission centered at 475 nm. This observation is in accordance with previous
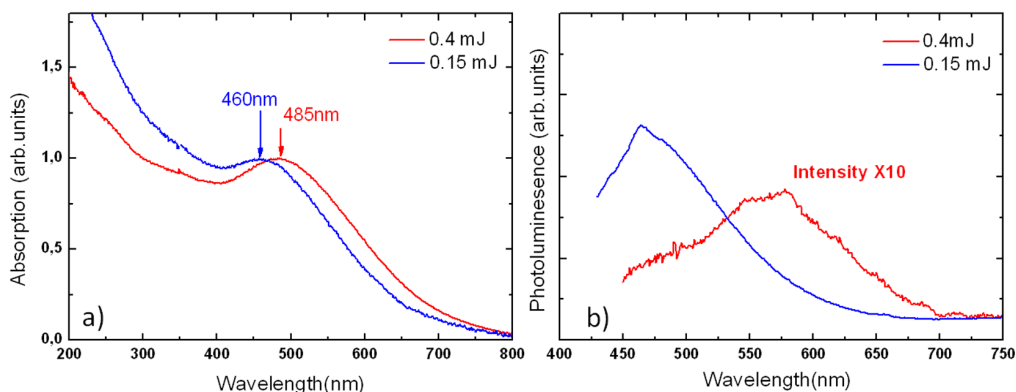
Fig. 2. Absorption (a) and photoluminescence (b) spectra of the Silicon nanoparticles prepared via femtosecond laser ablation of a silicon target in deionized water at 0.4 mJ (red line) and 0.15 mJ (blue line) energy regime (excitation wavelength 400 nm).

works reporting for the luminescence properties of small Si-NPs [10,21]. On the other hand, the Si-NPs colloidal solution prepared in the high energy regime, displays a red-shifted PL emission with a peak maximum at 575 nm and a decrease in intensity with respect to the PL observed in the low energy regime. The observed trend is connected to mean size and size dispersion of the nanoparticle present in solution. It is known that the photoluminescence peak of Si-NPs redshift as the nanoparticle mean size increases due to quantum confinement effect [22] which occurs when NPs size is comparable to the Bohr radius of the exciton, or larger. Three distinct categories of quantum confinement have been identified from strong regime to weak regime according to the relative value of the bohr radius and nanoparticle size [22]. In the case of colloidal solution prepared at lower energy, the mean size of generated Si-NPs is 5 ± 3 nm as reported from the histogram of particle size (Fig. 1(b)). Taking into account the value of 4.9 nm of exciton Bohr radius for silicon, the intense photoluminescence of Si-NPs colloidal solution is assumed to arise from carriers recombination carriers in a strong confinement regime. On the other hand, in the case of colloidal solution prepared at higher fluence, the nanoparticle mean size is around 65 nm with high size dispersion varying from 10 nm to 120 nm. So, in this case the nanoparticle size is larger than the exciton Bohr radius value and luminescent Si-NPs are considered to be in a weak confinement regime, with a lower energy band gap and therefore a red-shifted emission. The lower photoluminescence intensity observed results from the wide size dispersion of the nanoparticle: the larger the size dispersion, the lowest the PL intensity [22]. Based on these observations, we conclude that small nanoparticle produced at lower energy are more suitable candidate for imaging applications, as we will see in section 3.3.

After investigating the fluorescence and absorption properties on the particles, the quantum yield (Q.Y.) of the Si-NPs was determined by comparison with a Q.Y. standard (freshly prepared solution of Alexa 405 in deionized water; Q.Y. 54%), using the following formula: $\Phi NP = \Phi Standard$ (gradNP/gradStandard)(nNP^2/nStandard^2) [23] with Φ being the Q.Y., grad the gradient (slope) of the plot of the integrated fluorescence intensity vs. absorbance and n the refractive index of the solvent (1.33 in our case for deionized water). Samples of Si-NPs in water were put into 1 cm quartz cuvettes and diluted until the absorbance was below 0.15. At least three samples of different concentration were prepared. The absorbance of the standard was adjusted to be equal to each NP dispersion at the excitation wavelength. Figure 3 is reported the plot of the integrated fluorescence intensity vs. absorbance for alexa 405 Dye (black dots) and Si-NPs (red dots). For clarity of the figure, integrated fluorescence intensity was multiplied by a factor 100. The quantum yield of Si-NPs colloidal solution is determined to be around 0.1%. 1 to 2% QY has been reported to be sufficient for cell labeling studies [24].
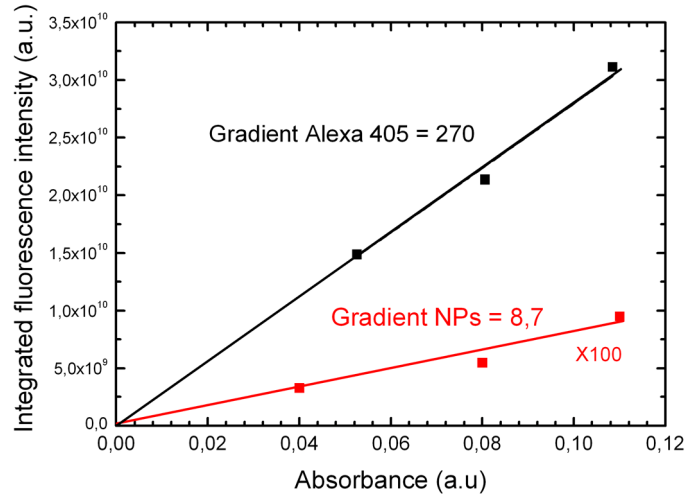
Fig. 3. Integrated fluorescence intensity vs absorbance for alexa 405 Dye (black dots) and Si-NPs (red dots).

3.3 Productivity analysis

The NPs productivity, via PLAL has been investigated in the past revealing its dependence with many parameters such as laser system (laser pulse energy, repetition rate) and thickness of the liquid above the target [25,26]. It has been reported that with the use of an appropriate laser system and optimized parameters, a gram/hour scale nanoparticle production rate can be achieved allowing to envisage potential mass production by laser ablation [26]. Usually, the NPs productivity is estimated by evaluation of the target mass lost after laser processing. In some cases, the value was deducted from a linear extrapolation of the ablated materials amount obtained after a short irradiation time considering any laser-nanoparticle interactions or concentration effects [25]. In this work, we evaluated the NPs productivity estimating the Si atom concentration present in solution after ablation using ICP-EOS measurements. Then the number of Si-NPs were calculated manually based on NPs average diameter estimated from TEM analysis. The evaluation of the NPs productivity was made for the colloidal solution of ultra-small Si-NPs (< 10 nm) since they are promising candidate for bio-imaging applications. Figure 4 shows representative plots of absorption properties and the corresponding NPs productivity of the colloidal solution. In Fig. 4(a) is reported the absorption spectra of Si-NPs colloidal solution obtained at different irradiation time in the low energy regime. The absorption peak intensity located at 460 nm, i.e. indicating generation of small Si-NPs (< 10nm), is found to increase with the irradiation time due to an increase of the NPs productivity. In Fig. 4(b) is reported the Si atom concentration obtained at different irradiation time estimated by ICP-EOS and the corresponding calculated number of nanoparticle (red squares). At least three amounts of each solution has been analyzed for statistic revealing a low data dispersion. The Si atom concentration generated in solution is found to increase with irradiation time. The value varies from 4 µg to 14 µg from 15 to 90 min, indicating a productivity rate of 0.136 µg/min. The number of NPs produced has been estimated taking into account a NP size of 5.5 nm (Fig. 1(b)) and it was found in the range of 10^{13} NPs per ml. Parameters of NP productivity are summarized in Table 1. Further experiments are in progress to scale up the NP productivity, by decreasing the liquid thickness above target surface and by increasing the energy pulse together with the spot size on the target surface in order to keep constant the energy/surface ratio (i.e. energy density) for the efficient generation of ultra-small Si NPs (size less than 10 nm).
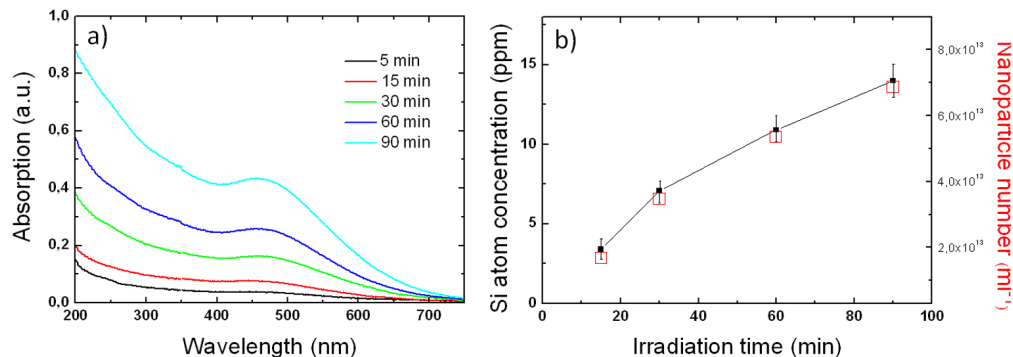
Fig. 4. (a) Absorption spectra of silicon nanoparticle synthesized by PLAL in the low energy regime for different irradiation time (b) Si atom concentration present in solution after laser processing evaluated by ICP-EOS measurement as a function of irradiation time (black square) and the corresponding calculated number of particles (red square).

Table 1. Summarized Results on the Productivity of Si-NPs Prepared by PLAL in the Low Energy Regime

Irradiation time (min)	Absorption intensity[a] (a.u.)	Si Atom concentration[b] ($\mu g.ml^{-1}$)	NP concentration[c] (ml^{-1})
15	0.075	3.4	1.67E13
30	0.162	7.1	3.47E13
60	0.257	10.9	5.35E13
90	0.431	14.1	6.87E13

[a] Absorption intensity value was taken at the peak maximum. [b] From ICP-EOS measurements. [c] Calculated taking into account a mean NP size of 5.5nm.

3.4 Fluorescence microscopy imaging

In order to underline the potential applications of Si-NPs prepared via PLAL method as fluorescent probe [27], fluorescence microscopy imaging was carried as shown in Fig. 5. It displays the fluorescence images collected by excitation at 405nm, in the configuration of (a) full spectral range and (c) selected spectral range. Here, drop-casted samples show a coffee ring with the NPs concentration occurring from the borders to the centre. Various PL measurements at different locations have been made. In Fig. 5(a) is reported a spectral image acquired on the ring border and in Fig. 5(b), the PL spectra relative to two different region of interest. It is evident how the PL spectrum of the NPs is in good agreement with a size dispersion lower than 10nm. NP emits in the blue-violet range with a peak emission around 475 nm, as previously reported. This observation indicates that agglomeration effects like ripening or fusion of the nanoparticles does not occur after drop casting deposition which is suitable for further labeling applications. On the other hand as expected no PL emission (red spectrum) is observed on the glass slide as a background spectrum. Identical measurement has been carried out for Si-NPs colloidal solution with mean size of 65 nm, no imaging has been recovered due to their less efficient luminescence emission.
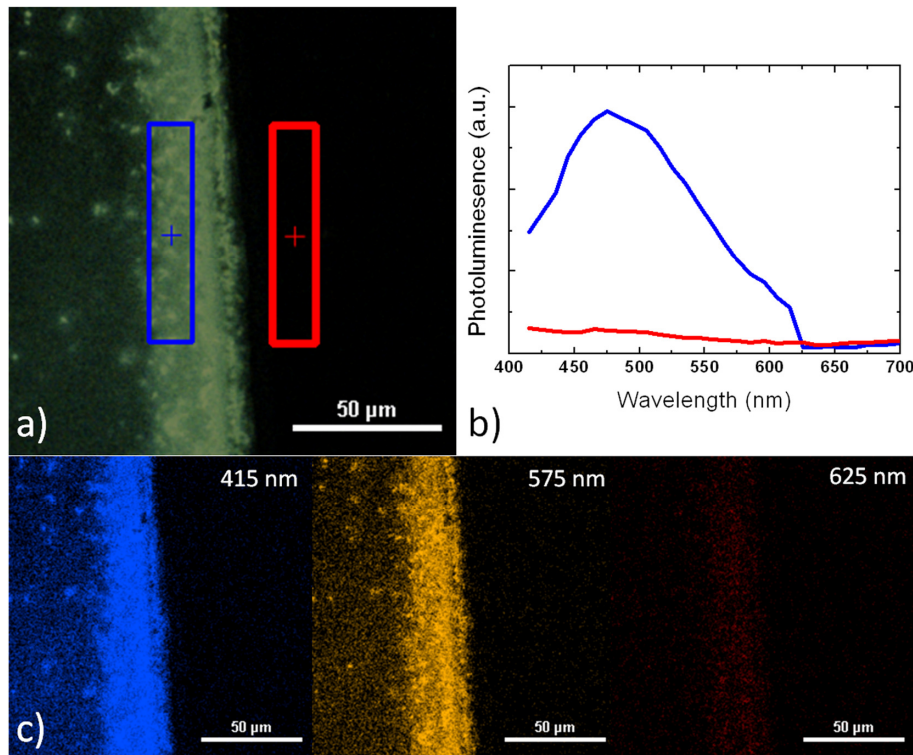
Fig. 5. Fluorescence imaging microscopy of silicon nanoparticles prepared via PLAL method in the low energy regime. (a) Spectral image acquired on the ring border and (b) the PL spectra relative to two different region of interest. Color of the PL spectra corresponds to the color used in the covered area in the optical image. (c) Selection of channels centered at 3 different wavelength.

4. Conclusion

We have reported about a simple but effective technique for generating luminescent silicon quantum dots in colloidal solution form and investigated their photoemissive properties towards imaging applications. Silicon nanoparticles have been synthesized by laser ablation of Silicon bulk in deionized water avoiding the use of reduction agents or chemical precursors, suitable for biomedical applications. Successful fabrication of silicon nanoparticles has been confirmed by UV-Vis spectroscopy together with TEM analysis. The absorption peak located at 460 nm and 480 nm is consistent with a population of average size of 5 nm and 65 nm, respectively. A new method for evaluating NPs productivity has been reported by measuring via ICP technique the Si atom concentration present in solution after laser processing. It is also demonstrated by photoluminescence spectroscopy that Si nanoparticles are good emitters in the visible range. The small and large Si nanoparticle show peak emission in the blue i.e., 475 nm and red range, i.e., 575 nm. Si nanoparticles with a size less than 10 nm, have been demonstrated by fluorescence imaging microscopy technique, to be good candidate for imaging applications.